Accepted Manuscript

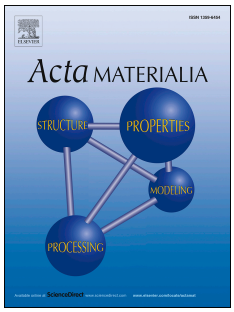

In-situ observation of evolving microstructural damage and associated effective electro-mechanical properties of PZT during bipolar electrical fatigue

Wei Lin Tan, Katherine T. Faber, Dennis M. Kochmann

PII: S1359-6454(18)30875-9

DOI: https://doi.org/10.1016/j.actamat.2018.10.065

Reference: AM 14943

To appear in: *Acta Materialia*

Received Date: 6 August 2018

Revised Date: 29 October 2018

Accepted Date: 31 October 2018

Please cite this article as: W.L. Tan, K.T. Faber, D.M. Kochmann, In-situ observation of evolving microstructural damage and associated effective electro-mechanical properties of PZT during bipolar electrical fatigue, *Acta Materialia*, https://doi.org/10.1016/j.actamat.2018.10.065.

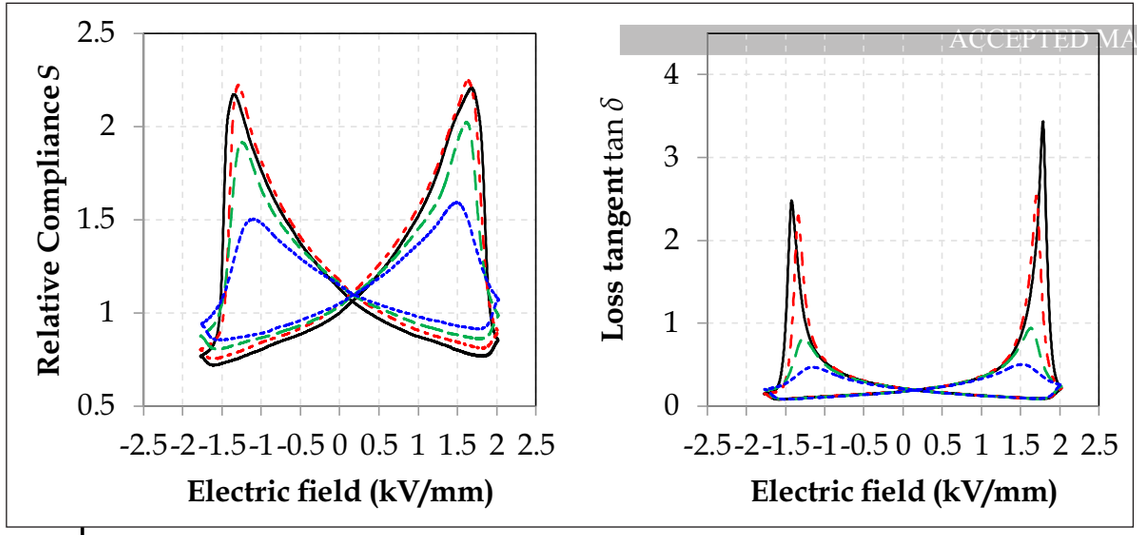

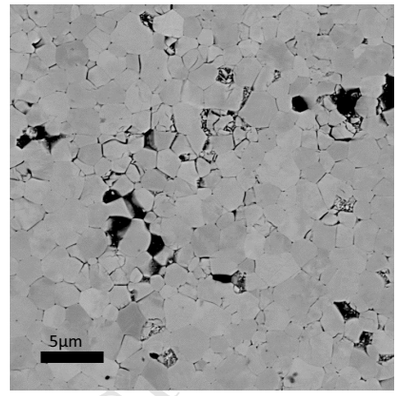

ferroelectric fatigue:

mechanical fatigue
vs.
electrical fatigue

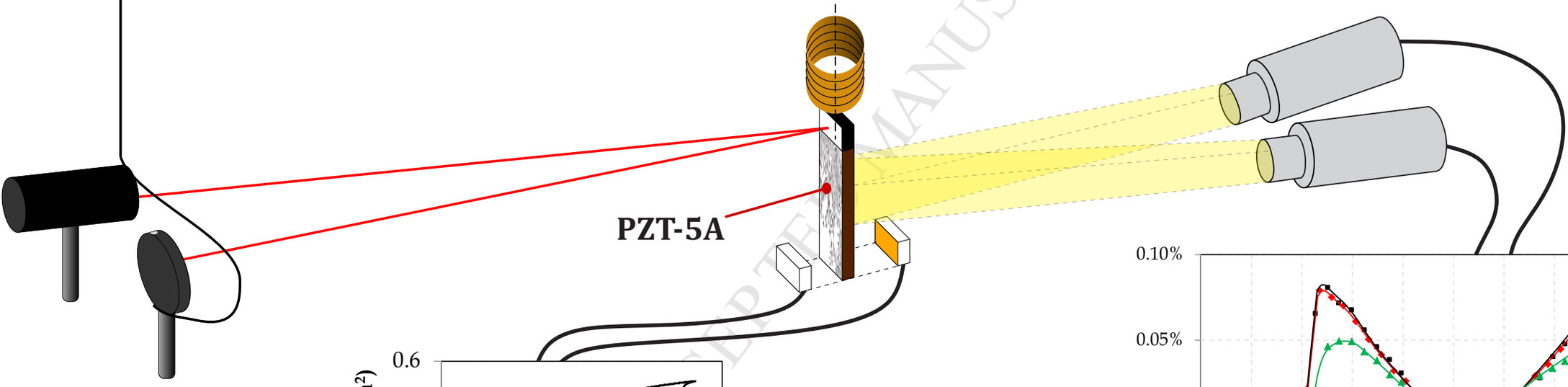

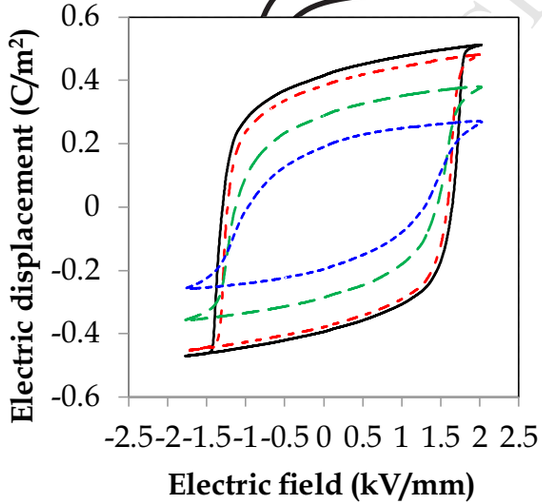

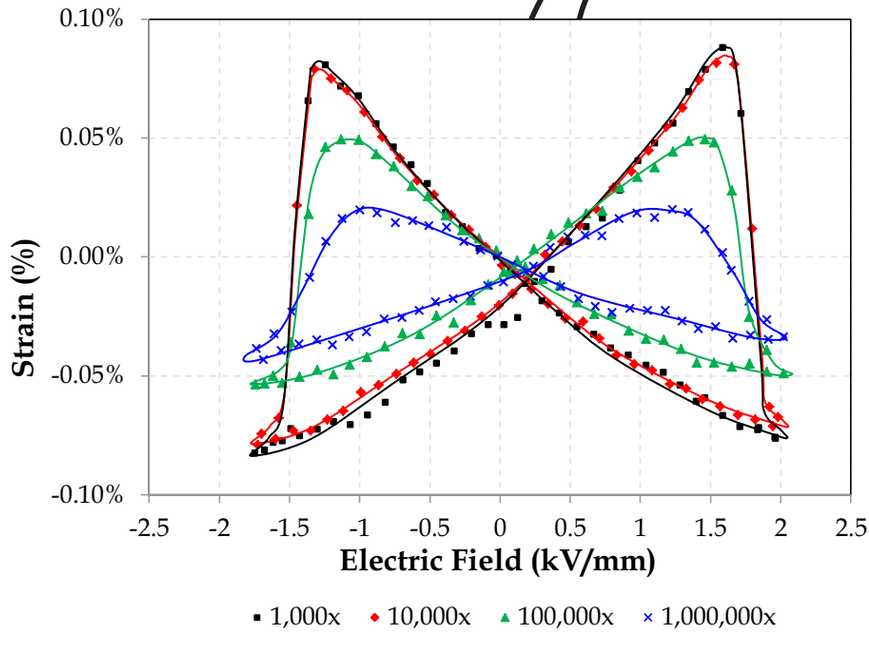

In-situ observation of evolving microstructural damage and associated effective electro-mechanical properties of PZT during bipolar electrical fatigue

Wei Lin Tan[a], Katherine T. Faber[a], Dennis M. Kochmann[a,b,*]

[a]*Division of Engineering and Applied Science, California Institute of Technology, Pasadena, CA 91125, U.S.A.*
[b]*Mechanics & Materials, Department of Mechanical and Process Engineering, ETH Zürich, 8092 Zürich, Switzerland*

Abstract

We investigate the fatigue behavior of bulk polycrystalline lead zirconate titanate (PZT) during bipolar electric field cycling. We characterize the frequency- and cycle-dependent degradation in both the effective electro-mechanical properties (specifically, the electrical hysteresis and the macroscopic viscoelastic stiffness and damping measured by Broadband Electromechanical Spectroscopy, BES) and the microstructural damage evolution (quantified via scanning electron microscopy). The BES setup enables the mechanical characterization while performing electrical cycling so as to measure the evolving viscoelasticity without remounting the sample; particularly measuring the viscoelastic damping allows us to gain insight into the ferroelectric domain wall activity across the full electric hysteresis and over the full range of cycles. A clear dependence on the electric cycling frequency is observed in the rates of degradation of all measured properties including an up to 10% increase in dynamic compliance and a 70% decrease in electric displacement magnitude. We quantify the evolving micro-crack density across wide ranges of numbers of cycles and compare with changes in the effective compliance. Interestingly, the observed strong degradation in the ferroelectric hysteresis is contrasted by relatively mild changes in the effective viscoelastic moduli, while samples clearly indicate increasing levels of micro-damage.

Keywords: ferroelectricity, electro-mechanical coupling, polycrystal, fatigue

1. Introduction

Polycrystalline lead zirconate titanate ($Pb[Zr_xTi_{1-x}]O_3$, or PZT) is ubiquitous in actuators, sensors and memory devices due to its superior piezoelectric and ferroelectric properties [1–3]. During operation such components are frequently subjected to sustained cyclic electrical and mechanical loading, which causes fatigue and an eventual degradation of the mechanical properties and device performance. Fatigue is especially detrimental during bipolar electrical loading, which prevents ferroelectric ceramics like PZT and barium titanate ($BaTiO_3$) from being more widely used for large strain actuation [4] as well as in memory applications and for set-and-hold actuation [1, 5].

Ferroelectric fatigue is a complex process since mechanisms of both mechanical and electrical fatigue are involved, and it manifests itself through changes to the material's microstructure as well as changes in the effective electro-mechanically-coupled performance [6]. Observable effects of bipolar electrical fatigue include (*i*) a decrease in amplitude of the polarization hysteresis loop indicating a loss in polarizability, (*ii*) a decrease in amplitude of the butterfly strain hysteresis implying a loss in ferroelectric actuation strain, (*iii*) macroscopic sample cracking especially near electrodes and interfaces, and (*iv*) micro-cracking within the bulk of the polycrystal preferably in an intragranular fashion [6–9]. While the latter have clear consequences on the mechanical material behavior, the creation of free surfaces also affects the distribution of electrical charges and thereby the ferroelectric performance. It is well-established that the progression of crack growth and mechanical damage depend strongly on the cycling frequency of the bias electric field, as is the evolution of the ferroelectric hysteresis and butterfly curve during fatigue. Even though those effects have been qualitatively observed [10–12], they have not been quantified in a systematic fashion.

*Phone +41 44 632 32 76
Email address: dmk@ethz.ch (Dennis M. Kochmann)

The origin of the effects of ferroelectric fatigue are collectively attributed to a decrease in domain switching capability with increasing numbers of cycles as well as macro- and micro-cracking within the body [13–16]. These effects are neither independent, nor have they thus far been quantified extensively. Chemical or structural causes of reduced domain switching include the pinning of domain walls at charged defects as well as at oxygen vacancies and other domain walls [11, 17–22], a decrease in nucleation sites for the formation of new domain walls [23, 24], development of internal fields [25–27] and internal damage leading to conductive corrosion paths [28]. Mechanical causes of fatigue include macro-crack formation and delamination (particularly near interfaces), micro-cracking within the body (especially along grain boundaries and regions of high internal stresses), as well as domain pinning due to mechanical stresses [5, 10, 12, 29].

It is experimentally challenging to isolate and observe the effects of any one of the aforementioned causal mechanisms. Nuffer et al. [7] employed acoustic emission to observe and classify domain switching in PZT (PIC 151) over 10^8 cycles at 50 Hz. Since acoustic emission events occur due to abrupt local stress or strain changes within a material, acoustic emission events of different amplitudes were attributed to 'difficult' and 'easy' domain wall motion, which occur at different applied electric fields and are affected by agglomeration of point defects. They also differentiated domain wall motion from micro-cracking events because the latter are two orders of magnitude higher in amplitude. However, that study did not quantify micro-cracking events during fatigue.

A proper quantification of the mechanical damage accrued during ferroelectric fatigue at different bipolar cycling frequencies can serve as the basis for differentiating domain wall pinning due to cracks or internal stresses versus domain wall pinning caused by point defects and chemical alterations of the material. Physics-based and phenomenological models for the evolution of mechanical fatigue in ferroelectrics due to bipolar electric field cycling have been developed by assuming growth of micro-cracks [30, 31], but thus far experimental validation of those models is sparse. Additionally, preliminary theoretical studies [32, 33] investigating the effect of micro-cracking on the decrease in polarization amplitude have shown that mechanical damage contributes to a polarization decrease, but this effect is over an order of magnitude smaller than the observed changes in polarization.

Here, we aim to add new qualitative and quantitative insight into the frequency-dependent ferroelectric fatigue of PZT-5A ($Pb[Zr_{0.52}Ti_{0.48}]O_3$). We use a combination of Broadband Electromechanical Spectroscopy (BES) [34], 3D Digital Image Correlation (3D-DIC), and statistical analysis of micro-cracks using scanning electron microscopy (SEM) to isolate and quantify the occurrence of micro-cracking as well as the degradation of the mechanical properties of PZT-5A during bipolar electrical fatigue at various cycling frequencies. BES allows for the simultaneous application of low-frequency high-voltage electrical cycling and high-frequency contactless mechanical vibrational excitation. The former serves to characterize the electrical hysteresis and, in combination with 3D-DIC, the butterfly curve vs. the number of electric cycles. The latter enables the measurement of the dynamic compliance and viscoelastic damping throughout the electrical hysteresis after selected numbers of electric cycles, thus capturing changes in mechanical properties as well as a decrease in microstructural ferroelectric switching since the measured damping correlates with the kinetics of domain wall motion [35]. The remainder of this investigation is structured as follows. Section 2 summarizes the experimental methods, followed by a presentation and discussion of results in Section 3, before Sections 4 and 5, respectively, discuss and conclude this study.

2. Materials and Methods

2.1. Material Samples

We characterize the microstructure as well as the ferroelectric and viscoelastic properties of lead zirconate-titanate (PZT-5A) beam specimens (H × W × T = 38 mm × 3 mm × 1 mm) obtained from Piezo Systems, Inc. (Woburn, MA, USA). As-obtained samples were poled through-thickness with an an average grain size of ∼2 μm (as found by SEM inspection). For electrical testing, samples had sputtered nickel electrodes covering their two largest, opposite faces.

2.2. Broadband Electromechanical Spectroscopy (BES)

We measure the electrical and viscoelastic properties the PZT-5A samples using a setup of Broadband Electromechanical Spectroscopy (BES) [34, 35], schematically shown in Figure 1. Beam specimens are clamped at the base by

electrically isolated grip electrodes through which a triangle waveform bipolar electric field is applied with a peak-to-peak amplitude of 3.8 kV/mm across the sample's thickness (for reference, the coercive field of the as-received PZT-5A is 1.18 kV/mm [36]). Connected to a Sawyer-Tower circuit, the electrodes also serve to measure the total electric displacement in terms of accumulated surface charges. Knowledge of the thus obtained average electric displacement and the applied bias electric field yields the electrical hysteresis, which is characterized at electric-field cycling frequencies from 0.2 Hz to 10 Hz. A permanent magnet (neodymium-boron-iron, 6.35 mm × 6.35 mm × 2.54 mm, 12 N maximum pull) is attached to the sample's top end via a stiff Macor® clamp. By enclosing the magnet by a pair of vertical magnetic coils (driven electronically at 100 Hz AC), we exert an oscillating transverse force on the beam's tip in a contactless fashion, resulting in beam bending [37]. By choosing the vibrational frequency significantly higher than the electrical cycling frequency (yet sufficiently lower than the natural frequency of the beam sample to avoid resonance), we aim for a decoupling of the mechanical and electrical measurements; i.e., while the bias electric field slowly traverses the full electrical hysteresis approximately quasistatically, fast mechanical vibrations are used to extract the viscoelastic response at each point on the electrical hysteresis. To quantify the viscoelastic properties, a HeNe laser is reflected off the beam's tip by a mirror attached to the magnet clamp and onto a split-diode position sensor whose signal is fed into a lock-in amplifier to determine its amplitude and phase lag (with respect to the vibrational driver). The resulting signals admit characterizing the dynamic compliance and the damping (in terms of the loss tangent) of the specimen [38]. All viscoelastic measurements are taken at 0.1 Hz electric field cycling after a stabilization period of six cycles to reduce any kinetic effects on the measured electro-mechanical data [35]. That is, even though electric cycling is performed at different frequencies, those frequencies are temporarily changed to 0.1 Hz for the duration of each viscoelastic characterization. Since specimens are tested over large numbers of electric cycles, changing the electric-cycling frequency for only a few cycles in order to obtain clean viscoelastic measurements is expected to not significantly affect the overall response. Furthermore, all measurements are performed in air to allow for full-field strain measurements via Digital Image Correlation (described below). It was verified that differences in viscoelastic measurements taken in air vs. vacuum are negligible for bending at 100 Hz. To investigate the fatigue behavior, each sample is cycled electrically between 10^5 to 10^6 times while recording the above information (with viscoelastic measurements taken only at selected numbers of cycles without interrupting the electrical cycling and without remounting the sample).

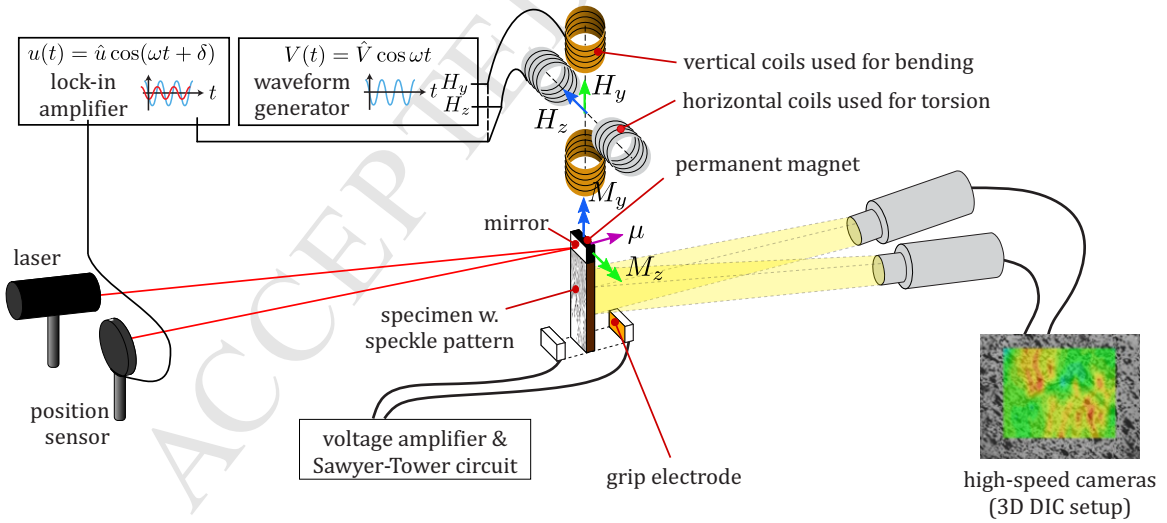

Figure 1: Schematic of the combined Broadband Electromechanical Spectroscopy (BES) and 3D Digital Image Correlation (DIC) setup. While 3D-DIC is used to extract the permanent strain in the sample for construction of the ferroelectric butterfly curve, BES is used to characterize the effective viscoelastic properties and the ferroelectric hysteresis across each electric cycle.

2.3. 3D Digital Image Correlation (3D-DIC)

Three-dimensional Digital Image Correlation is used to obtain full-field, contactless strain measurements of the specimen during electrical cycling. Two high-speed cameras (IL5 from Fastec Imaging, San Diego, CA, USA) are used for imaging at 25 frames per second for a duration of 12.5s for each data point, and images are processed using VIC-3D v.8 (Correlated Solutions, Inc., Irmo, SC, USA) to obtain the in-plane strain and out-of-plane displacement on the sample's back surface. Samples are spray-coated with a black and white speckle pattern, which is used to identify changes in displacements during loading [39].

In the cantilever beam configuration chosen here to admit vibrational viscoelastic measurements, we use 3D-DIC in order to differentiate the in-plane strains from the effects of out-of plane movement of the sample which causes an apparent change in strain of similar magnitude. We note that the strain component thus obtained and reported in the subsequent butterfly curves is perpendicular to the direction of the applied electric field, whereas most reported strain data in the literature are parallel to the applied electric field. Nevertheless, those two remanent strain components are crystallographically coupled, so that the same qualitative conclusions may be drawn.

2.4. Micro-Crack Statistics

2.4.1. Scanning Electron Microscopy (SEM)

In addition to samples fatigued for the full 10^5 to 10^6 cycles, we also investigate the evolution of micro-cracking by electrically cycling specimens up to intermediate numbers of cycles, followed by determining micro-crack statistics on images obtained from scanning electron microscopy (ZEISS 1550VP Field Emission SEM). Samples used for ex-situ micro-crack analysis must be prepared with care so as not to introduce additional cracks during the preparation process. For each sample, the nickel coating is removed via hand polishing using alumina polishing paper followed by four hours of vibro-polishing using colloidal silica. Unlike typical polishing and etching procedures using HF, colloidal silica vibro-polishing does not etch pristine, uncracked grain boundaries or differentially etch domains within a grain. This yields a low surface roughness with high topographic contrast in micro-cracked regions. Polished surfaces are imaged using SEM in backscattered electron mode (BSE) at 10 kV with 7000× magnification at a working distance of 7.3mm. BSE gives high contrast from cracked regions, which allows for automated edge detection of micro-cracks and cataloging of crack length and density for quantitative statistics. Figure 2 shows a representative SEM image of a fatigued PZT sample with clearly visible grain boundaries, some ferroelectric domains, voids and cracks. Cracks were cataloged automatically using ImageJ's *Analyze Particle* function (size: 30-Infinity pixels, circularity: 0.0-0.5) [40]. Eight images per sample were taken and independently evaluated to yield statistically representative data.

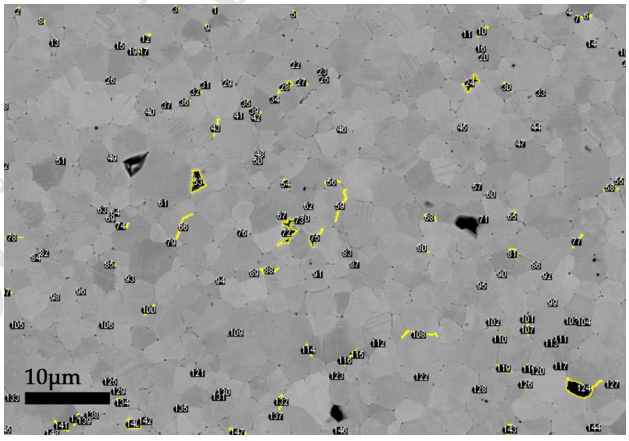

Figure 2: Representative SEM micrograph of micro-cracks in a fatigued PZT-5A sample with automatic edge recognition and size measurement for quantitative statistics.

2.4.2. Kachanov Model

In order to correlate the measured micro-crack density with macroscopic mechanical properties, homogenization models are a suitable avenue. A simple analytical homogenization of a cloud of micro-cracks to give the macroscopic compliance is the model by Kachanov [41], which assumes a cloud of planar micro-cracks of random orientations, embedded in an isotropic material. Here, we may approximate the polycrystalline, untextured bulk PZT as isotropic. However, micro-cracks along grain boundaries follow a tortuous path and their measured length is not equivalent to the length of a straight-line crack. We hence account for this tortuosity by establishing an effective length L_R, defined as the diameter of the circle which fully bounds each micro-crack. The macroscopic compliance S as a function of the micro-crack density is then approximated by

$$\frac{S}{S_0} = 1 + \frac{16\left(1-\nu_0^2\right)\left(1-\frac{3\nu_0}{10}\right)}{9\left(1-\frac{\nu_0}{2}\right)}\rho, \tag{1}$$

where the crack density ρ is defined by

$$\rho = \frac{1}{A}\sum_{i=1}^{n} L_{R_i}^2. \tag{2}$$

S_0 and ν_0 are the undamaged base material's compliance and Poisson's ratio (for isotropic polycrystalline PZT, $\nu_0 = 0.35$ as per vendor specification), A is the area of the image, and L_{R_i} is the length of the i-th crack (with n cracks in total).

3. Results

3.1. Evolution of the Electro-Mechanically Coupled Hystereses

Figure 3 shows representative hysteresis curves of electric displacement, relative dynamic compliance and relative damping for specimens cycled at 0.2, 1, 5 and 10 Hz. Curves obtained after 1, 10^4, 10^5 and 10^6 cycles are shown for each electric cycling frequency to highlight qualitative and quantitative changes in material behavior. Key trends evident from these curves include the following: (*i*) The polarization magnitude (i.e., the difference between positive and negative remanent polarization at zero applied electric field) decreases with prolonged bipolar electrical cycling across all frequencies. (*ii*) The peak height of the relative compliance decreases with cycling across all frequencies. (*iii*) The peak height of the loss tangent decreases with cycling across all frequencies. (*iv*) The relative compliance at zero applied electric field (measured at the transition from negative to positive e-field) increases slightly with electric cycling across all frequencies. (*v*) The viscoelastic loss tangent at zero applied electric field does not change significantly with cycling.

Trends (*i*), (*ii*) and (*iii*) are attributed to the extent of domain switching induced either electrically, mechanically or both, while trends (*iv*) and (*v*) reflect the base material property at zero applied electric field where no domain switching occurs. To further characterize the differences in degradation behavior at different electric field cycling frequencies, we track the above five parameters continually over the course of 10^5 to 10^6 cycles for each electric cycling frequency.

3.2. Electrical Hysteresis

As a standard metric for establishing electrical degradation in ferroelectrics during fatigue, we track the polarization hysteresis curve height at an applied electric field of $E = 0$ kV/mm. As Figure 4 shows, the decrease in polarization magnitude (and thus in polarizability) occurs most rapidly at lower cycling frequencies and approaches a lower tail-off than at higher frequencies. The curves showing the polarization magnitude also appear to converge with decreasing cycling frequencies, where the difference between the 1 Hz and 5 Hz trend is smaller than the difference between the 5 Hz and 10 Hz, while 0.2 Hz[1] behaves very similarly to 1 Hz.

[1] We chose to conduct experiments in air to enable the combined use of BES and 3D-DIC, which unfortunately results in mechanical sample failure especially at low frequencies; therefore, the 0.2 Hz data in Figure 4 end prematurely upon sample failure after close to 10^5 cycles.

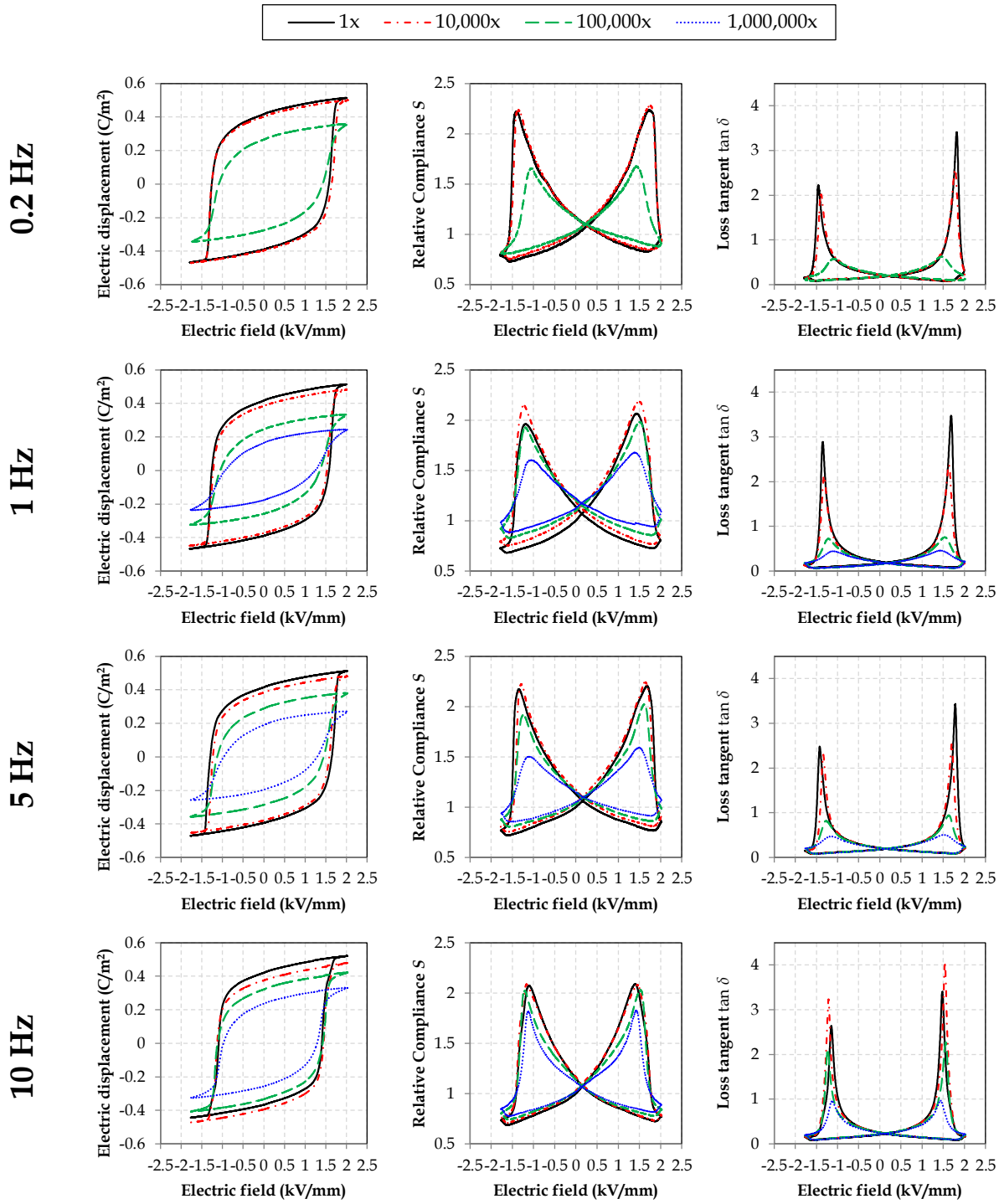

Figure 3: Broadband Electromechanical Spectroscopy (BES) hysteresis curves of electric displacement (*left column*), relative compliance S (*middle column*) and normalized loss tangent $\tan\delta$ (*right column*) for different electric cycling frequencies, measured after 1, 10^4, 10^5 and 10^6 cycles.

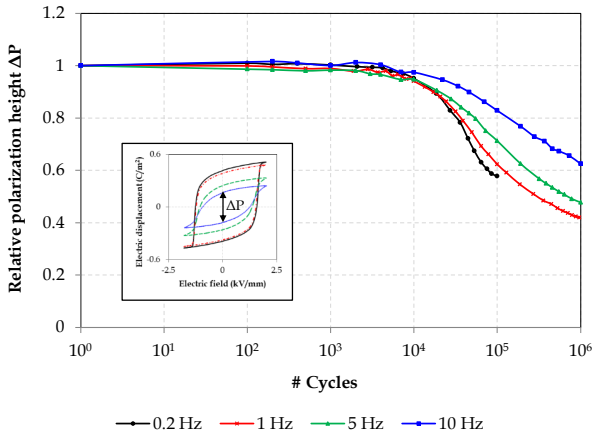

Figure 4: Relative polarization magnitude (i.e., height of the electric hysteresis loop at 0 kV/mm applied electric field) over 10^6 cycles of bipolar electrical fatigue for electric cycling frequencies of 0.2 – 10 Hz.

The observed decrease in polarization magnitude is a well-known phenomenon of bipolar electrical fatigue, which is often attributed to the agglomeration of point defects and the resulting obstruction of domain wall motion [11, 17–21]. The frequency dependence of the rate of degradation has also been observed before in various ferroelectric ceramics [11, 12, 42], and it is believed to be due to kinetic limitations. At higher frequencies, full switching may not occur, which reduces internal mechanical damage caused by lattice mismatch during 90°-switching. High frequencies also slow down the migration of charged defects, which in turns slows down the aggregation of point defects and hence delays the degradation of the polarization arising from domain wall pinning. This is consistent with the observation that at lower frequencies below 5 Hz (where full switching is achieved) the change in rate of degradation between one frequency and the next decreases and the reported data eventually appear to converge.

3.3. Viscoelastic Properties

It has been shown [35] that ferroelectric ceramics exhibit changes in viscoelastic properties when undergoing electric field cycling. In particular, the mechanical compliance and damping both peak near the coercive field, which has been attributed to, respectively, the mechanically induced domain switching and the dissipative effects of domain wall motion during ferroelectric switching. Specifically, as the electric hysteresis is traversed slowly by the applied electric field, the high-frequency vibrations admit characterizing mechanical damping which is tied to mechanisms of internal friction (here, of domain switching kinetics). Changes in the measured loss tangent are hence linked to ferroelectric switching activity and can thus provide information about the inhibition of ferroelectric switching as a consequence of fatigue, independent of any signs of mechanical fatigue. In order to assess both the mechanical changes and the dissipative effects of domain wall motion, we here track the compliance at $E = 0$ kV/mm, further the peak compliance, the loss tangent at $E = 0$ kV/mm, and the peak damping over 10^5 to 10^6 cycles for different electric cycling frequencies.

3.3.1. Dynamic Compliance

Peaks in dynamic compliance occur close to the coercive field because a small additional mechanical load can easily overcome the energy barrier between domain orientations and induce domain switching. When a bending moment is applied, the side of the specimen in tension switches into a vertical *a*-domain structure perpendicular to the applied electric field direction, while the side in compression switches into a horizontal *c*-domain structure parallel to the applied electric field. This mechanically induced domain switching increases the magnitude of bending of the specimen, manifesting as an apparent increase in dynamic compliance.

Figure 5a shows the change in peak relative compliance with cycling at different electric field frequencies. The shaded yellow region indicates the extent of machine noise relative to the measured signal. Similar to trends in polarization magnitude, the peak relative compliance remains fairly stable until 10^4 cycles before dropping steeply

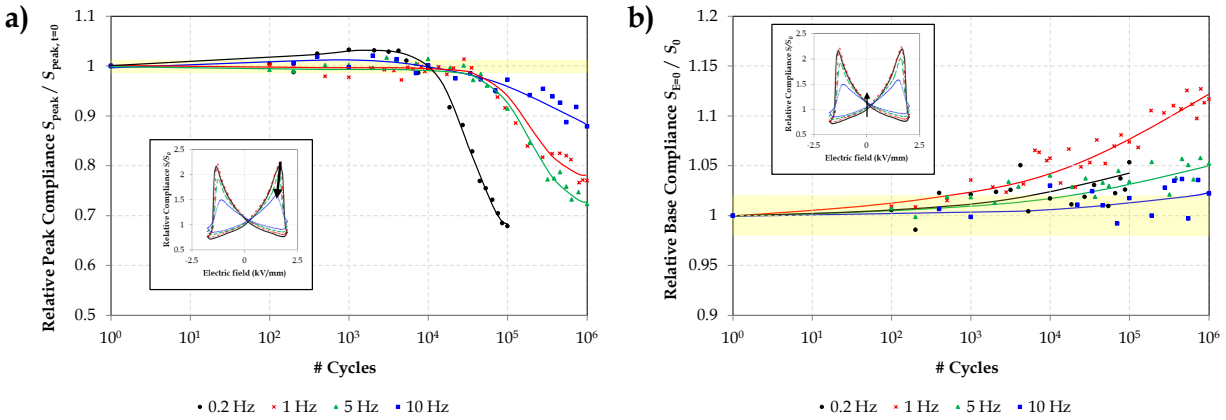

Figure 5: a) Relative peak compliance and b) relative base compliance at $E = 0$ kV over 10^6 cycles of bipolar electrical fatigue at electric cycling frequencies of 0.2 – 10 Hz. In both figures, the shaded yellow region represents the magnitude of machine noise relative to data.

(depending on electric cycling frequency), then plateauing as it approaches 10^6 cycles. Note that this drop in peak relative compliance is approximately half that of the decrease in polarization magnitude. Additionally, the shapes of the curves differ significantly for 10 Hz and 0.2 Hz, and the lower frequencies do not converge. These differences suggest that, although both polarization magnitude and peak relative compliance are related to the extent of domain switching, the former is primarily a function of changes in electrical properties in the ceramic while the latter is more closely related to the mechanical properties; hence, the nature of their fatigue behavior differs.

The base dynamic compliance taken at $E = 0$ kV/mm is indicative of changes in the mechanical properties of the specimen independent of domain switching phenomena. A primary cause for changes in compliance in ceramics is the occurrence of macro- and micro-cracking [43]. Figure 5b shows that the base dynamic compliance of the specimen without applied electric field increases by more than 10% over 10^6 cycles of electric field loading at 1 Hz, likely due to micro-mechanical damage accumulating over time. Higher frequencies of electric loading yield smaller increases in compliance, with 5 Hz increasing by approximately 5% and 10 Hz by only about 2%. These trends suggest that greater mechanical degradation occurs for lower electrical cycling frequencies, similar to the higher electrical property degradation at lower cycling frequencies observed via polarization magnitude in Section 3.2. The lowest frequency measurements do not appear to follow this trend, likely due to complications from holding a high *e*-field for long durations, which damages the specimen non-uniformly close to and away from clamped regions. We note that the changes in mechanical base compliance (Figure 5b) are significantly smaller than those of the switching-related peak compliance (Figure 5a).

3.3.2. Damping

Damping, i.e., the loss tangent (denoted by $\tan\delta$), is a measure of mechanical energy absorption through internal friction mechanisms [44]. Peaks in damping are observed close to the coercive field and occur due to the energy absorbed by mechanically induced domain switching during mechanical vibrations. Figure 6a shows the change in peak damping with cycling at different electric field frequencies. Peak damping degradation trends once again mirror those of the polarization magnitude and relative compliance, with higher frequencies exhibiting less degradation. However, the decrease in energy absorption is of much greater magnitude than either polarization magnitude or relative compliance, decreasing to <30% of its original state after 10^6 cycles. This dramatic decrease suggests that mechanically induced domain switching suffers more greatly from the effects of fatigue than does electrically induced domain switching.

The base damping taken at $E = 0$ kV/mm measures the mechanical energy absorption in the specimen independent of domain switching phenomena. At zero applied electric field, no additional absorption of mechanical energy due to domain switching is expected to occur. Figure 6b shows the relative change in base damping of the specimen at $E = 0$ kV/mm. There is a moderate change of ±5% over 10^6 cycles. However, as damping is very low, this scatter lies within the noise margin as shown by the shaded region. This small change in damping at zero electric field with

little to no cycling frequency dependence is consistent with the understanding that energy absorption occurs due to mechanically induced domain switching, which is absent at $E = 0$ kV/mm.

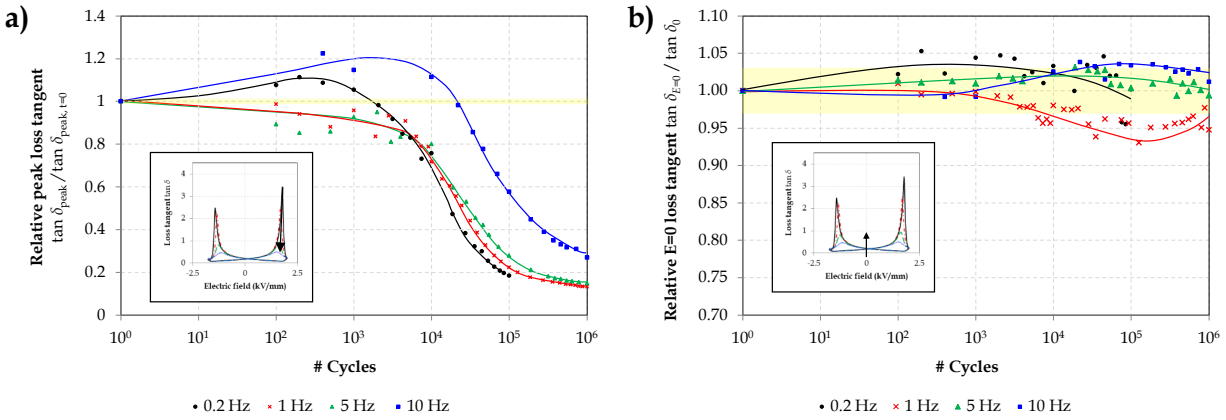

Figure 6: a) Relative peak damping and b) relative base damping at $E = 0$ kV/mm over 10^6 cycles of bipolar electrical fatigue at electric cycling frequencies of 0.2 – 10 Hz. The shaded yellow region represents the magnitude of noise relative to the data.

3.4. Strain Hysteresis

The ϵ_{yy}-strain hysteresis ('butterfly') curves obtained from DIC for electrical cycling at 5 Hz is shown in Figure 7a for 10^3, 10^4, 10^5 and 10^6 cycles. As with the hysteresis curves of the other electromechanical properties shown in Figure 3, the magnitude of the strain hysteresis decreases with cycling. This change in strain is due to ferroelastic switching, so this trend is consistent with other indicators of a reduction in domain switching during fatigue. As these measurements were taken without mechanical loading of the specimen, the domain switching underlying this data is purely electrically induced.

The magnitude of strain change per cycle is measured and plotted in Figure 7b for 0.2, 5 and 10 Hz. Shapes and trends of the strain magnitude fatigue curves exhibit significant similarity to the polarization magnitude fatigue curves (see Figure 4), and both sets of curves exhibit similar magnitudes of decrease ranging from 40 – 60% after 10^6 cycles. This is consistent with the understanding that both properties originate from purely electrically induced domain switching and are directly related to each other crystallographically.

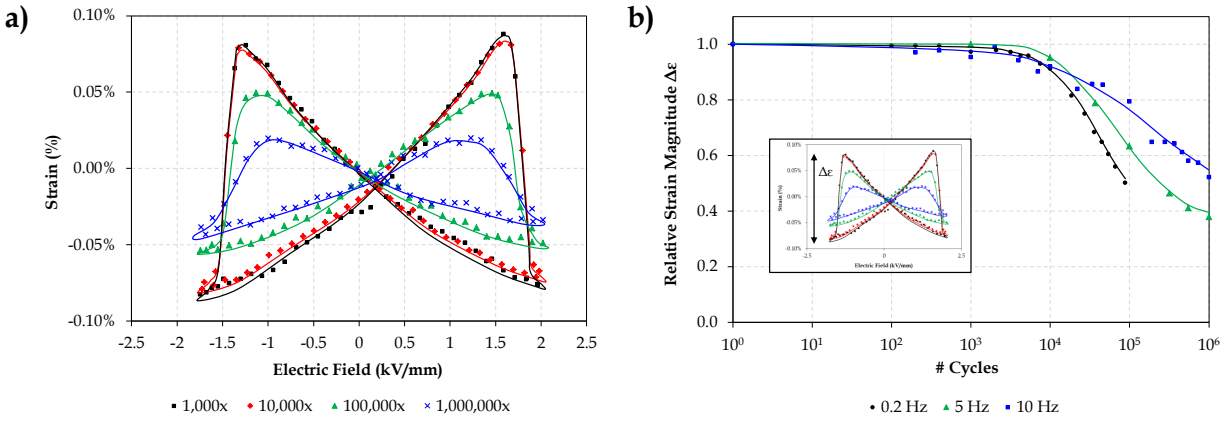

Figure 7: (a) In-plane y-direction (vertical relative to beam) strain hysteresis curves after different numbers of electric cycles for the representative electric cycling frequency of 5 Hz; (b) evolution of the peak-to-peak strain magnitude over 10^6 cycles of bipolar electrical fatigue for all tested frequencies from 0.2 – 10 Hz.

3.5. Micro-Cracks

Figure 8 shows SEM micrographs of specimens (a) before and (b) after $2 \cdot 10^6$ cycles of fatigue. Micro-cracks appear to form primarily along grain boundaries, but examples of intra-granular fracture are also visible. Crack densities were measured using images of polished surfaces for 0, 10^4, 2×10^4, 10^5, 2×10^5 and 10^6 cycles, cycled electrically at 1 Hz and 10 Hz as representative frequencies. Figure 9 shows the relative crack density evolution for 1 Hz and 10 Hz cycling. Small fluctuations in early data points, in particular the apparent decrease between 0 and 10^4 cycles at 1 Hz, are due to sampling and have a T-test P-value of 0.961, and thus are not statistically different.

Both show an increase in crack density, with the slower 1 Hz cycling exhibiting a larger (7%) increase in crack density while the faster 10 Hz cycling only shows a 4% increase. This difference is consistent with macroscopic BES measurements which suggest that lower-frequency fatigue results in higher levels of degradation both electrically and mechanically.

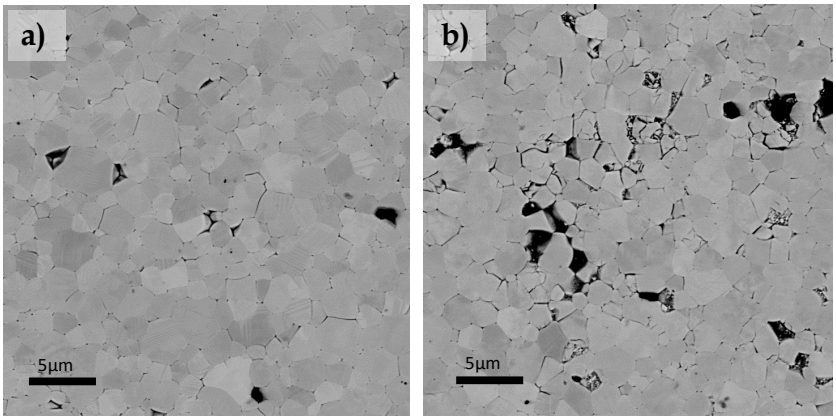

Figure 8: a) Polished surface of an as-received, pre-poled PZT specimen, b) polished surface of a PZT specimen after 2×10^6 bipolar electrical cycles at 1 Hz.

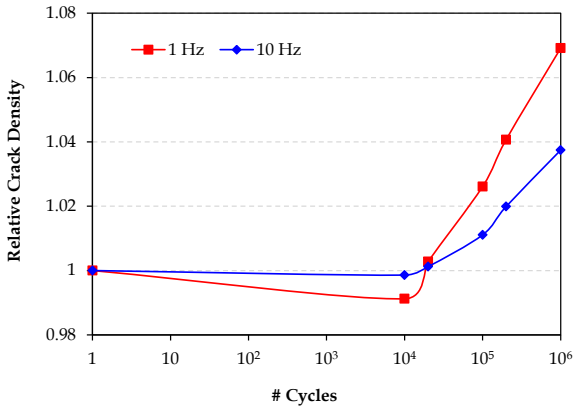

Figure 9: Comparison of the relative crack density evolution during fatigue for the two representative cases of 1 Hz and 10 Hz bipolar electrical cycling.

4. Discussion

Our BES and DIC measurements as well as micro-crack statistics are aimed at shedding light onto the impact of mechanical fatigue (primarily manifesting in micro-crack and void formation on the microscale of the brittle ceramic) versus electrical fatigue (stemming from a combination of mechanisms that include domain wall pinning, chemical alterations, and charge accumulation). While both fatigue phenomena occur simultaneously and in a coupled fashion, they affect the measured properties in different ways, which is why the presented data help improve our understanding of the domain switching behavior and crack growth during bipolar electric field cycling of ferroelectric ceramics. In the following sections, we first establish a correlation between the measured mechanical compliance data and the formation of micro-cracks, followed by a discussion of the evolution of electrical vs. mechanical fatigue.

4.1. Micro- vs. Macroscale Mechanical Properties

In order to quantify the mechanical damage that occurs due to electric cycling, we have tackled the problem from both the macroscopic scale and the microscopic scale. On the one hand, using BES we have obtained macroscopic data of the base viscoelastic properties (viz., compliance and damping) of the entire specimen at $E = 0$ kV/mm while fatigue is progressing. On the other hand, by terminating the electric field cycling after various intermediate numbers of cycles, we have measured the evolving micro-crack density. Using the model described in Section 2.4, we can independently calculate and anticipate the decrease in the macroscopic compliance based on the increasing concentration of micro-cracks. Figure 10 shows the comparison between the two compliance metrics, viz. the macroscopic BES measurements and the microstructurally-informed, calculated compliance based on the measured micro-crack density for two representative frequencies. The magnitudes of change as well as the slopes of both methods are in convincing agreement, suggesting that the macroscopic changes in dynamic compliance are, to a large extent, indeed due to bulk micro-cracking and not any other effect which could potentially alter the compliance, such as changes in domain structure or purely surface and electrode-interface macro-cracking. The presented compliance data thus allow us to interpret the changes in mechanical properties during fatigue with good confidence.

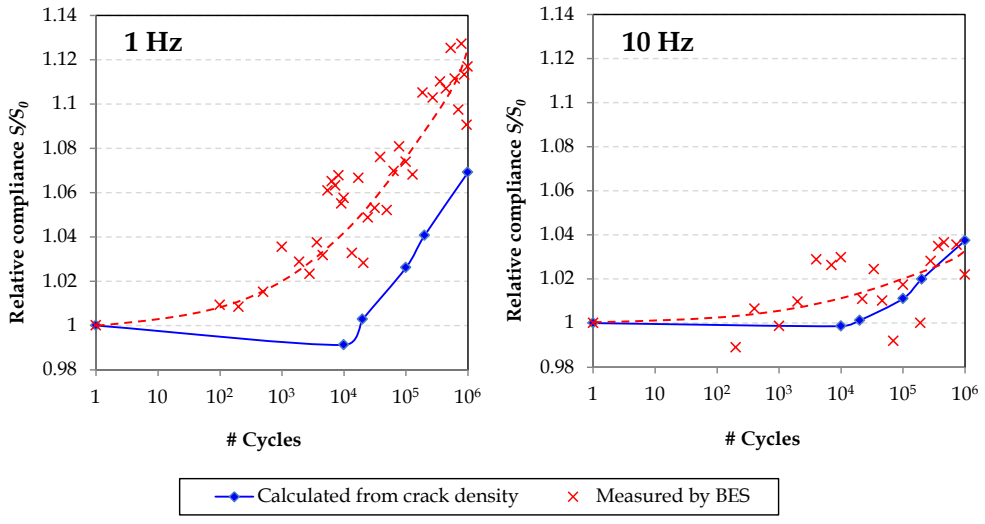

Figure 10: Comparison of the normalized compliance $S_{E=0}/S_0$ measured via BES at $E = 0$ kV/mm (*red cross markers*) and the relative compliance calculated from the micro-crack statistics (*blue diamond markers*) at electric field cycling frequencies of 1 Hz (*left*) and 10 Hz (*right*). The shown relative compliance data are normalized by the respective base values during the first cycle.

4.2. Domain Switching

The magnitude of the polarization hysteresis over time has been the most common proxy to describe fatigue in ferroelectrics. It indicates the degree of domain switching occurring and has a well-established logarithmic decrease

with cycling, which we have verified via the BES measurements in Figure 4. Wojnar et al. [35] argued that the strong increase in mechanical compliance and damping near the coercive field are similarly due to domain switching. Our simultaneous BES measurements of the polarization, peak dynamic compliance, and peak damping at various times during electric cycling (as shown in Figures 4, 5 and 6, respectively) confirm a remarkable similarity in the time evolution of these three properties. This indeed suggests a common underlying cause and corroborates the argument that the motion of domain walls changes the viscoelastic properties of the ferroelectric under varying electric field, most pronounced when close to the coercive field where domain wall mobility is highest. For all three measured properties, a lower electric cycling frequency leads to a steeper and larger overall decrease in each property. For the polarization and strain magnitudes, the effect of further lowering the cycling frequency below 5 Hz diminishes quickly, suggesting that electrically induced domain switching kinetics occurs on a similar timescale that is independent of the cycling frequency in this slow, quasistatic regime. By contrast, the peak compliance and peak damping trends differ from those polarization and strain trends in both magnitude and shape, which supports the hypothesis that both properties are associated with mechanically induced domain switching instead. While lower-frequency cycling appears to degrade more quickly, there is no clear trend of convergence for the peak compliance in the quasistatic limit, since, e.g., the 0.2 Hz peak compliance data decreases more rapidly than those reported for 1 and 5 Hz. This suggests that – unlike electrical fatigue whose signs tends to converge in the low-frequency limit – a different mechanical degradation mechanism becomes dominant at low frequencies (or that the specimen is mechanically degraded non-uniformly at lower frequencies). Since we could isolate the purely mechanical effects of fatigue through the $E = 0$ kV/mm viscoelastic properties of the specimen (which correlate with the ex-situ micro-crack density measurements, as shown in Section 4.1), it is natural to conclude that micro-cracking is responsible for the mechanical degradation and that the latter is hence more sensitive to frequency in the low-frequency range.

We note that the peak compliance data also exhibit a small increase in peak height until about 10^4 cycles before decreasing logarithmically. The mechanism for this small increase is unclear but could be a result of the interplay between micro-crack formation and increasing alignment of the domain structure of grains resulting in more mechanically induced domain switching.

4.3. Base Viscoelastic Properties

In order to quantify the effect of mechanical degradation on the overall decrease in ferroelectric performance of the specimen, we examine the change in the base (i.e., $E = 0$ kV/mm) viscoelastic properties of the specimen, as described in Section 3.3. Figure 5b shows a clear increase of the dynamic compliance with time across all electric loading frequencies, which is in agreement with the formation of micro-cracks during bipolar electric cycling, hypothesized to be due to internal stresses caused by strain mismatch across grains during domain switching. In general[2], the measured compliance appears to increase faster for lower frequencies, which could be due to more complete domain switching increasing the internal mechanical stresses and hence generating more micro-cracking. Low frequencies are also more likely to result in charge build-up and internal discharge, which also triggers cracking. We note that damping at $E = 0$ kV/mm remains within the level of noise throughout cycling (see Figure 6b), which verifies that mechanically induced domain switching does not occur far from the coercive field, and that any changes in internal stresses do not cause significant changes in internal friction of the ceramic material.

5. Conclusions

Viscoelastic and electrical properties of PZT-5A were measured in-situ during bipolar electrical loading at 0.2, 1, 5 and 10 Hz. The hysteresis curves of polarization, compliance, damping and strain showed significant degradation over 10^6 cycles, with higher frequencies degrading less than lower frequencies. Polarization magnitude and strain magnitude, both associated with electrically induced domain switching, decreased by 40-60%. Properties arising from mechanically induced domain switching such as the peak compliance decreased by 10-30%, while the peak damping (associated with the domain wall kinetics) decreased by 80-90%. While attribution of causes of domain

[2]We note that, as discussed before, the results at 0.2 Hz electric cycling frequency deviate from some of the trends discussed here for the viscoelastic properties. This was attributed to complications associated with applying large *e*-fields over long times, which damages the specimen non-uniformly close to and away from clamped regions.

switching degradation was not possible, the extent of mechanical damage could be accurately quantified by correlating macroscopic dynamic compliance and micro-crack density evolution, which showed good agreement and confirmed that compliance changes during fatigue were primarily due to micro-cracking. Interestingly, results indicate that electrical fatigue (i.e., the degradation of domain switching processes as seen in the changes of the polarization magnitude and strain amplitude as well as in the peak damping indicative of domain switching activity) converges to a low-frequency limit that is independent of electric cycling frequency, whereas mechanical fatigue (surfacing in the measured compliance data and supported by SEM crack counting) strongly depend on frequency even in the low-frequency limit. This hints at separate mechanisms at play, which may guide further (particularly micro-scale) experimentation as well as model development. We note that our study did not probe the micro-mechanical effects of domain wall pinning, defect agglomeration, oxygen vacancies and other chemical effects; we cannot assess to what extent each of those individually contributes to the decrease in domain switching during fatigue.

Acknowledgments

W. L. Tan acknowledges support from the DSO National Laboratories Postgraduate Scholarship.

References

[1] K. Uchino, Piezoelectric Actuators and Ultrasonic Motors, Springer US, 1997.
[2] G. H. Haertling, Ferroelectric ceramics: History and technology, Journal of the American Ceramic Society 82 (4) (1999) 797–818. doi:10.1111/j.1151-2916.1999.tb01840.x.
URL http://dx.doi.org/10.1111/j.1151-2916.1999.tb01840.x
[3] H. Takasu, The ferroelectric memory and its applications, Journal of Electroceramics 4 (2-3) (2000) 327–338. doi:10.1023/A:1009910525462.
URL https://doi.org/10.1023/A:1009910525462
[4] E. Burcsu, G. Ravichandran, K. Bhattacharya, Large electrostrictive actuation of barium titanate single crystals, Journal of the Mechanics and Physics of Solids 52 (4) (2004) 823 – 846. doi:http://dx.doi.org/10.1016/j.jmps.2003.08.001.
URL http://www.sciencedirect.com/science/article/pii/S0022509603001315
[5] C. Lynch, L. Chen, Z. Suo, R. Mcmeeking, W. Yang, Crack growth in ferroelectric ceramics driven by cyclic polarization switching, Journal of Intelligent Material Systems and Structures 6 (2) (1995) 191–198. doi:10.1177/1045389X9500600206.
URL https://doi.org/10.1177/1045389X9500600206
[6] D. C. Lupascu, Fatigue in Ferroelectric Ceramics and Related Issues, Springer, Berlin Heidelberg, 2004.
[7] J. Nuffer, D. Lupascu, J. Rödel, Damage evolution in ferroelectric PZT induced by bipolar electric cycling, Acta Materialia 48 (14) (2000) 191–198. doi:10.1016/S1359-6454(00)00173-7.
URL https://doi.org/10.1016/S1359-6454(00)00173-7
[8] N. Balke, H. Kungl, T. Granzow, D. C. Lupascu, M. J. Hoffmann, J. Rödel, Bipolar fatigue caused by feid screening in pb(zr,ti)o_3 ceramics, Journal of the American Ceramic Society 90 (12) (2007) 3869–3874. doi:10.1111/j.1551-2916.2007.02041.x.
URL https://onlinelibrary.wiley.com/doi/full/10.1111/j.1551-2916.2007.02041.x
[9] S. Zhukov, J. Glaum, H. Kungl, E. Sapper, R. Dittmer, Y. Genenko, H. v. Seggern, Fatigue effect on polarization switching dynamics in polycrystalline bulk ferroelectrics, Journal of Applied Physics 120 (6) (2016) 064103. doi:10.1063/1.4960691.
URL https://doi.org/10.1063/1.4960691
[10] J. Shieh, N. Fleck, J. Huber, Observation of fatigue crack growth in ferroelectrics under electrical loading, Vol. 4699, 2002, pp. 4699 – 4699 – 13. doi:10.1117/12.475016.
URL https://doi.org/10.1117/12.475016
[11] L. Zhou, N. Zhang, A. Zimmerman, F. Aldinger, L. Li, Frequency dependent electric fatigue in antiferroelectric pzst ceramics, Ferroelectrics 315 (1) (2004) 61–71. doi:10.1080/00150190590933005.
URL https://doi.org/10.1080/00150190590933005
[12] W. Promsawat, N. Promsawat, S. Jiansirisomboon, O. Namsar, F. Marlton, J. Daniels, S. Pojprapai, Investigation of frequency effect on electrical fatigue and crack tip domain-switching behaviors in $Pb(Mg_{1/3}Nb_{2/3})_{0.65}Ti_{0.35}O_3$ ceramics via synchrotron X-ray diffraction, Journal of the European Ceramic Society 37 (15) (2017) 4609–4616. doi:10.1016/j.jeurceramsoc.2017.06.020.
URL https://doi.org/10.1016/j.jeurceramsoc.2017.06.020
[13] J. K. Shang, X. Tan, A maximum strain criterion for electric-field-induced fatigue crack propagation in ferroelectric ceramics, Materials Science and Engineering: A 301 (2) (2001) 131 – 139. doi:https://doi.org/10.1016/S0921-5093(00)01812-8.
URL http://www.sciencedirect.com/science/article/pii/S0921509300018128
[14] L. Zhenhua, G. Julia, G. Torsten, J. Wook, D. Robert, H. Mark, R. Jrgen, Bipolar and unipolar fatigue of ferroelectric bnt-based lead-free piezoceramics, Journal of the American Ceramic Society 94 (2) (2011) 529–535. doi:10.1111/j.1551-2916.2010.04101.x.
URL https://onlinelibrary.wiley.com/doi/abs/10.1111/j.1551-2916.2010.04101.x
[15] H. Hinterstein, J. Rouquette, J. Haines, P. Papet, J. Glaum, M. Knapp, J. Eckert, M. Hoffman, Mechanisms of aging and fatigue in ferroelectrics, Physics Review B 90 (9) (2014) 094113. doi:10.1103/PhysRevB.90.094113.
URL https://doi.org/10.1103/PhysRevB.90.094113

[16] Y. Genenko, J. Glaum, M. Hoffmann, K. Albe, Mechanisms of aging and fatigue in ferroelectrics, Materials Science and Engineering: B 192 (1) (2015) 52–82. doi:10.1016/j.mseb.2014.10.003.
URL https://doi.org/10.1016/j.mseb.2014.10.003

[17] U. Robels, G. Arlt, Domain wall clamping in ferroelectrics by orientation of defects, Journal of Applied Physics 73 (1993) 3454. doi:10.1063/1.352948.
URL https://doi.org/10.1063/1.352948

[18] C. Brennan, Model of ferroelectric fatigue due to defect/domain interactions, Ferroelectrics 150 (1) (2010) 199–208. doi:10.1080/00150199308008705.
URL https://doi.org/10.1080/00150199308008705

[19] A. Kontsos, C. M. Landis, Computational modeling of domain wall interactions with dislocations in ferroelectric crystals, International Journal of Solids and Structures 46 (6) (2009) 1491–1498. doi:http://dx.doi.org/10.1016/j.ijsolstr.2008.11.021.
URL http://www.sciencedirect.com/science/article/pii/S0020768308004939

[20] T. Rojac, M. Kosec, B. Budic, N. Setter, D. Damjanovic, Strong ferroelectric domain-wall pinning in $BiFeO_3$ ceramics, Journal of Applied Physics 108 (2010) 074107. doi:10.1063/1.3490249.
URL https://doi.org/10.1063/1.3490249

[21] H. Guo, X. Liu, J. Rödel, X. Tan, Nanofragmentation of ferroelectric domains during polarization fatigue, Advanced Functional Materials 25 (1) (2015) 270–277. doi:10.1002/adfm.201402740.
URL https://doi.org/10.1002/adfm.201402740

[22] Z. Fan, X. Tan, In-situ TEM study of the aging micromechanisms in a $BaTiO_3$-based lead-free piezoelectric ceramic, Journal of the European Ceramic Society 38 (10) (2018) 3472 – 3477. doi:https://doi.org/10.1016/j.jeurceramsoc.2018.03.049.
URL http://www.sciencedirect.com/science/article/pii/S095522191830195X

[23] A. Tagantsev, I. Stolichnov, Injection-controlled size effect on switching of ferroelectric thin films, Applied Physics Letters 74 (1999) 1326. doi:10.1063/1.123539.
URL https://doi.org/10.1063/1.123539

[24] W. Zhang, K. Bhattacharya, A computational model of ferroelectric domains. Part I: model formulation and domain switching, Acta Materialia 53 (1) (2005) 185–198, read 04/25/13. doi:http://dx.doi.org/10.1016/j.actamat.2004.09.016.
URL http://www.sciencedirect.com/science/article/pii/S1359645404005580

[25] M. Ozgul, S. Trolier-McKinstry, C. A. Randall, Influence of electrical cycling on polarization reversal processes in $Pb(Zn_{1/3}Nb_{2/3})O_3$-$PbTiO_3$ ferroelectric single crystals as a function of orientation, Journal of Applied Physics 95 (8) (2004) 4296–4302. doi:10.1063/1.1687046.
URL https://doi.org/10.1063/1.1687046

[26] M. Ozgul, S. Trolier-Mckinstry, C. A. Randall, Fatigue induced effects on bipolar strain loops in pzn-pt piezoelectric single crystals, Journal of Electroceramics 20 (3) (2008) 133–138. doi:10.1007/s10832-007-9120-8.
URL https://doi.org/10.1007/s10832-007-9120-8

[27] S. Zhukov, S. Fedosov, J. Glaum, T. Granzow, Y. A. Genenko, H. von Seggern, Effect of bipolar electric fatigue on polarization switching in lead-zirconate-titanate ceramics, Journal of Applied Physics 108 (1) (2010) 014105. doi:10.1063/1.3452326.
URL https://doi.org/10.1063/1.3452326

[28] H. Duiker, P. Beale, J. Scott, Fatigue and switching in ferroelectric memories: Theory and experiment, Journal of Applied Physics 68 (11) (1990) 5783. doi:10.1063/1.346948.
URL https://doi.org/10.1063/1.346948

[29] H. Cao, A. Evans, Electric-field-induced fatigue crack growth in piezoelectrics, Journal of the American Chemical Society 77 (7) (1994) 1783–1786. doi:10.1111/j.1151-2916.1994.tb07051.x.
URL https://doi.org/10.1111/j.1151-2916.1994.tb07051.x

[30] I. Arias, S. Serebrinsky, M. Ortiz, A phenomenological cohesive model of ferroelectric fatigue, Acta Materialia 54 (4) (2006) 975–984. doi:10.1016/j.actamat.2005.10.035.
URL https://doi.org/10.1016/j.actamat.2005.10.035

[31] S. Lange, A. Ricoeur, High cycle fatigue damage and life time prediction for tetragonal ferroelectrics under electromechanical loading, International Journal of Solids and Structures 80 (1) (2016) 181–192. doi:10.1016/j.ijsolstr.2015.11.003.
URL https://doi.org/10.1016/j.ijsolstr.2015.11.003

[32] S. Kim, Q. Jiang, Microcracking and electric fatigue of polycrystalline ferroelectric ceramics, Smart Materials and Structures 5 (3) (1996) 321. doi:10.1088/0964-1726/5/3/010.
URL https://doi.org/10.1088/0964-1726/5/3/010

[33] K. Sze, N. Sheng, Polygonal finite element method for nonlinear constitutive modeling of polycrystalline ferroelectrics, Finite Elements in Analysis and Design 42 (2005) 107–129. doi:10.1016/j.finel.2005.04.004.
URL https://doi.org/10.1016/j.finel.2005.04.004

[34] J. B. Le Graverend, C. S. Wojnar, D. M. Kochmann, Broadband Electromechanical Spectroscopy (BES): Measuring the dynamic mechanical response of viscoelastic materials under temperature and electric-field control in a vacuum environment, J. Mater. Sci. 50 (10) (2015) 3656–3685. doi:10.1007/s10853-015-8928-x.
URL http://dx.doi.org/10.1007/s10853-015-8928-x

[35] C. S. Wojnar, J.-B. le Graverend, D. M. Kochmann, Broadband control of the viscoelasticity of ferroelectrics by electric fields, Appl. Phys. Lett. 105 (16) (2014) 162912. doi:10.1063/1.4899055.
URL http://dx.doi.org/10.1063/1.4899055

[36] M. W. Hooker, Properties of PZT-based Piezoelectric Ceramics Between-150 and 250C, Citeseer, 1998.

[37] R. Lakes, J. Quackenbusch, Viscoelastic behavior in indium tin alloys over a wide range of frequency and time, Philosophical Magazine Letters 74 (1996) 227–238.
URL http://silver.neep.wisc.edu/~lakes/gInSn.pdf

[38] R. S. Lakes, Viscoelastic measurement techniques, Review of Scientific Instruments 75 (4) (2004) 797–810. doi:10.1063/1.1651639.
[39] M. A. Sutton, Digital Image Correlation for Shape and Deformation Measurements, Springer US, Boston, MA, 2008, pp. 565–600. doi:10.1007/978-0-387-30877-7_20.
URL https://doi.org/10.1007/978-0-387-30877-7_20
[40] C. A. Schneider, W. S. Rasband, K. W. Eliceiri, NIH Image to ImageJ: 25 years of image analysis, Nature methods 9 (7) (2012) 671–675. doi:10.1038/nmeth.2089.
URL https://www.nature.com/articles/nmeth.2089
[41] M. Kachanov, Effective elastic properties of cracked solids: Critical review of some basic concepts, Applied Mechanics Reviews 45 (1992) 304–335. doi:10.1115/1.3119761.
URL https://doi.org/10.1115/1.3119761
[42] N. Zhang, L. Li, Z. Gui, Frequency dependence of ferroelectric fatigue in PLZT ceramics, Journal of the European Ceramic Society 21 (5) (2001) 677–681. doi:10.1016/S0955-2219(00)00248-X.
URL https://doi.org/10.1016/S0955-2219(00)00248-X
[43] W. H. Gu, K. T. Faber, Tensile behavior of microcracking SiC-TiB_2 composites, Journal of the American Ceramic Society 78 (6) (1995) 1507 – 1512. doi:10.1111/j.1151-2916.1995.tb08845.x.
URL https://onlinelibrary.wiley.com/doi/abs/10.1111/j.1151-2916.1995.tb08845.x
[44] R. Lakes, Viscoelastic Solids, CRC Mechanical Engineering Series, CRC Press, 1999.
URL http://books.google.com/books?id=soZZl17sm5IC